Polymer Testing 62 (2017) 254–262

Contents lists available at ScienceDirect

Polymer Testing

journal homepage: www.elsevier.com/locate/polytest

Product Performance

On the analysis of cut resistance in polymer-based climbing ropes: New testing methodology and resulting modes of failure

A. Andrés Leal [a, *], Rolf Stämpfli [b], Rudolf Hufenus [a]

[a] Laboratory for Advanced Fibers, Empa, Swiss Federal Laboratories for Materials Science and Technology, Lerchenfeldstrasse 5, 9014 St. Gallen, Switzerland
[b] Laboratory for Biomimetic Membranes and Textiles, Empa, Swiss Federal Laboratories for Materials Science and Technology, Lerchenfeldstrasse 5, 9014 St. Gallen, Switzerland

ARTICLE INFO

Article history:
Received 30 May 2017
Accepted 5 July 2017
Available online 8 July 2017

Keywords:
Rope
Elmendorf tear test
Pendulum test
Cut resistance
Scanning electron microscopy (SEM)

ABSTRACT

Rock climbing ropes tend to suffer catastrophic failure when dynamically loaded over a sharp edge. Seeking to gain a better understanding of this phenomenon, a testing methodology based on a pendulum tear tester has been developed to quantify the cut resistance of polymer-based core-sheath climbing ropes in a reliable and reproducible manner. Experimental measurements indicate that the specific energy required to cut a rope is directly proportional to the linear density of the sheath component in the rope, where a high coefficient of determination between the two parameters is observed. Field tests under actual rock climbing conditions involving a granite sharp edge confirm the practical relevance of the developed laboratory methodology. An analysis of failure modes by means of scanning electron microscopy indicates that cut resistance is inversely proportional to the amount of frictional heating introduced at the point of contact between rope and sharp edge.

1. Introduction

Polymer-based rock climbing ropes are composed of thousands of single polyamide 6 filaments which are hierarchically arranged into yarns and ply yarns with various yarn numbers. The rope construction, typically referred to as *kernmantle*, comprises a core of unidirectional strands surrounded by a sheath of braided strands. The core has primarily a load-bearing function, whereas the sheath fulfills multiple functions such as protecting the core from abrasion and dirt, while also contributing to the mechanical performance of the rope. Rock climbing ropes, also known as dynamic ropes, have a strain to failure in the order of 40% which allows stopping a climber's fall in a controlled manner, preventing a shock-related injury [1]. When a rope is stretched during a climber's fall, the filaments are subjected to tensile, bending and torsional deformations due to their helical arrangement [2], where friction between the different rope components plays a major role in energy dissipation [3]. Friction in ropes is the result of relative slip between components, where the slip and the contact pressure define the work done by friction in opposing a structure deformation [4]. Leech has identified various modes of friction in braided polymer fiber ropes, classified as friction between components or within components [4]. The friction between components can take the form of axial slip, twist slip, scissoring (the angle between the two sliding components reduces as tension is increased), or sawing (tangential slip) [4]. In addition, dilation and distortion of cross-sectional area in a rope component represent the types of friction within a component in a tensed rope [4]. The exertion of frictional forces during rope deformation leads to heat generation which in turn causes a temperature rise in the rope [5].

Dynamic climbing ropes typically do not fail in service unless they are dynamically loaded over a sharp object in the form of a cliff edge, a falling rock or a worn metallic carabiner [1]. There has been a significant effort invested in understanding the cut resistance of single filaments, yarns and ropes. Mayo and Wetzel have described that for a single fiber held in tension, transverse compression is likely to introduce local flaws such as cracks and kink bands which lead to progressive local tensile failure [6]. They further describe that, once a blade cuts between halfway to three quarters of the way through the fiber, the increased tension in the remaining fibrils leads to tensile failure [6]. Hudspeth et al. have illustrated the effect of punch geometry on the modes of failure of a clamped single fiber subjected to a transverse load [7]. They observed that a round indenter yields transverse failure strains comparable to the

* Corresponding author.
E-mail addresses: Andres.Leal@empa.ch (A.A. Leal), Rolf.Staempfli@empa.ch (R. Stämpfli), Rudolf.Hufenus@empa.ch (R. Hufenus).

http://dx.doi.org/10.1016/j.polymertesting.2017.07.004
0142-9418/

expected longitudinal tensile strain to failure, while the tested fiber ends were highly fibrillated, just as in the case of failure due to pure axial tension [7]. In contrast, cutting with a razor blade results in localized failure which is a consequence of the extremely high stress concentration induced at the blade-fiber interface [7]. At the yarn level, the cut resistance of yarns under tension has been studied by Shin et al., who found that higher axial pretensions lead to yarn breakage at lower cutting loads [8]. They observed that most fiber ends in the fractured yarn were bulbous, with a range of bulb sizes within the yarn [8]. Analyses of filaments extracted from partially cut yarns indicated that deformed material at the tip of the advancing blade flows opposite to the direction of cutting, leading to an accumulation of deformed polymer on the front side of the fiber [8].

Various researchers have developed experimental devices to evaluate the effect of different parameters on the dynamic properties of climbing ropes. Pavier used a falling trolley running on a vertical column to dynamically load a rope [9]. In order to perform the test, the rope is threaded through a fixed metal loop (carabiner) while one end of the rope is tied to the trolley, and the opposite end is secured by pneumatic grips. Once the trolley is released, free fall takes place until the rope is fully tensioned (Fig. 1a). Using carabiners with different radii, Pavier showed that, for a 8.7 mm diameter rope and falling mass of 70 kg, a reduction of carabiner radius leads to a decreased number of falls before the rope fails catastrophically (Fig. 1b) [9]. The fact that rope failure occurs at the point in contact with the heavily loaded carabiner during full extension has also been demonstrated by Rüedi et al., who used a 80 kg mass to quantify the effect of carabiner radius on number of falls endured by the rope (Fig. 1b) [10].

The sharp edge resistance of climbing ropes has been a research topic of particular interest for rope manufacturers and sports scientists. Using both laboratory and scale model setups, Blümel et al. have analyzed the sharp edge resistance properties of mountaineering ropes [11,12]. In the laboratory setup, they attached a series of weights to a rope which falls a distance of 0.8 m before contacting a granite sharp edge. Alternatively, the scale model setup makes use of a pendulum impact testing machine adapted with a notched steel blade which represents the sharp edge. Both experimental setups indicate clear linear correlations between the weight of the falling mass (laboratory setup) or cutting energy (scale model setup) and the variables rope diameter, and rope weight per meter [11,12].

Using the pendulum impact testing machine modified by Blümel et al., Bückers [13] evaluated the effect of pre-tensioning force on the cut resistance of a 10.3 mm diameter climbing rope, where an inversely proportional correlation was clearly observed (Fig. 2a). Further, Bückers also measured the energy required to cut cords and ropes of varying diameters, roughly confirming a directly proportional trend between rope diameter and specific cutting energy [13] (Fig. 2b). Bückers observed that the way in which the rope specimens are pre-tensioned during the cutting tests is an extremely critical factor, concluding that the manual pre-tensioning procedure followed by Blümel et al. [11,12] and by Bückers leads to significant uncertainties in the experimental results [13].

Based on all of the above, the purpose of the present work is to describe the development of a testing methodology which quantifies the cut resistance of polymer-based climbing ropes in a reliable and reproducible manner. The capability of the developed testing methodology to produce experimental results which are representative of real life rock climbing scenarios is confirmed by means of field tests. The failure modes of ropes from both laboratory and field test are analyzed and contrasted at the single filament level as a function of their location within the cut specimen.

2. Experimental

2.1. Materials

All dynamic climbing ropes under analysis were produced and supplied by Mammut Sports Group AG. The ropes are made of polyamide 6 filaments, arranged in the form of a core of unidirectional strands engulfed by a sheath of braided strands, where each strand is composed of yarns and ply yarns with various yarn numbers. The ropes were subjected to hydrophobic coatings [14] which are proprietary and not disclosed by the manufacturer. The physical characteristics of relevance for the present study are listed in Table 1. Rope diameters were determined according to DIN EN 892 [15] as follows: rope specimens were clamped in a universal testing machine with a gauge length of 1200 mm and a load of 10 kg. The rope was allowed to relax for 4 min while maintaining the 10 kg force before its diameter was measured at three points 100 mm apart. The reported values represent mean values.

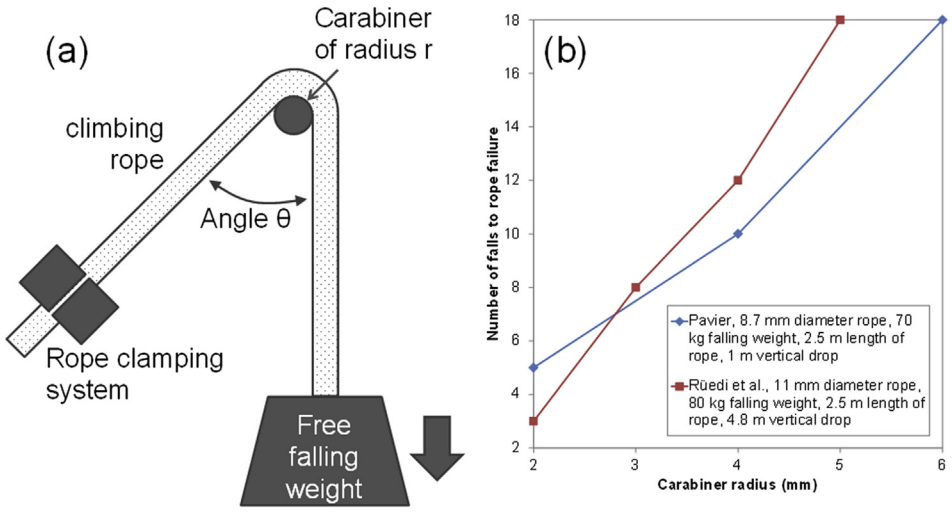

Fig. 1. (a) Schematic illustration (not to scale) of dynamic free-falling weight test to determine the number of falls that a rope withstands before catastrophic failure; (b) number of falls to rope failure as a function of metal loop (carabiner) radius reported by Pavier [9] and by Rüedi et al. [10]. The lines joining the data points in Fig. 1b serve only as a visual aid.

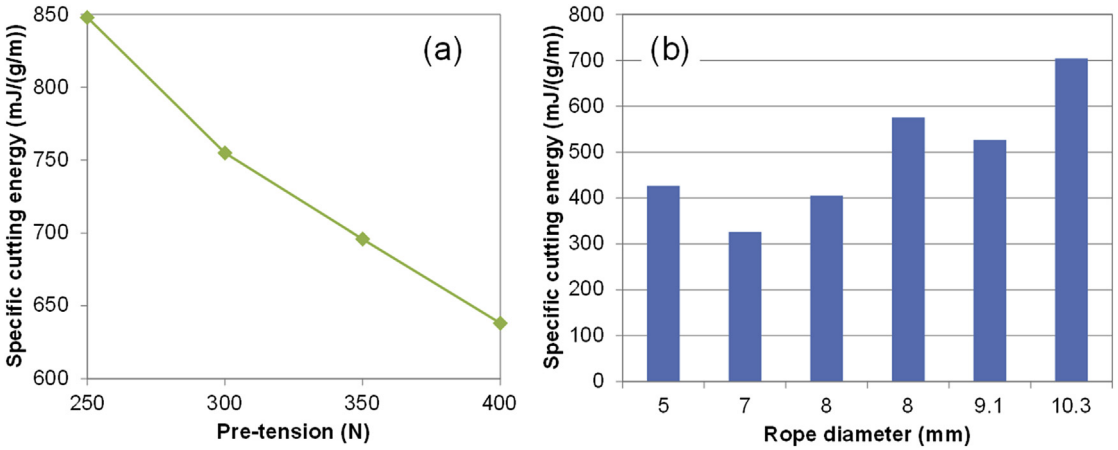

Fig. 2. (a) Effect of pre-tensioning force on the energy needed to cut a 10.3 mm diameter rope; (b) correlation between specimen diameter and specific cutting energy (pre-tension 350 N). Tests carried out with a modified pendulum impact testing machine [13]. The lines joining the data points in Fig. 2a serve only as a visual aid.

Table 1
Physical properties of dynamic climbing ropes used in the analysis of cut resistance.

Diameter (mm)	Linear density of the rope (g/m)	Linear density of the sheath component (g/m)
8.7	51.2	18.5
9.2	57.4	20.7
9.5 (i)	60.6	23.7
9.5 (ii)	60.5	24.1
9.7[a]	61.4	24.0
9.8	64.1	24.0
10.1	68.2	24.1
10.2	70.8	29.4

[a] The hydrophobic coating applied to the 9.7 mm rope differs from that of all other ropes under analysis.

2.2. Modified pendulum tester for cut resistance performance of climbing ropes

The main parts of the test rig (Fig. 3a) are a universal tensile testing machine (type Z100 RetroLine, Zwick Roell GmbH, Ulm, Germany) with hydraulic rope clamps and a modified Elmendorf tear tester pendulum (type FX3700, TEXTEST Instruments, Schwerzenbach, Switzerland). The original clamps of the tear tester were removed and replaced by a blade (Fig. 3c) consisting of a 55° thread cutting tool (type 0/1-K55-N-TiN, Ifanger AG, Uster, Switzerland). The 55° steel blade had a radius of 0.07 mm and the surface is TiN coated to prevent wear. In order to simulate a cutting movement that mimics the sliding of the rope over a sharp, tilted edge, the blade was mounted at an angle of 35° to the direction of movement of the pendulum. Since the ropes have an elongation at 10 kN tension ranging from about 35% up to 60%, an additional support (stop bar in Fig. 3a and b) was installed to limit the rope deflection during contact with the blade. The following settings were used: clamping length of 460 mm, clamping force up to 250 bar, pre-tension of 10 kN, maximum cutting energy 8.26 J (9600 cN weight).

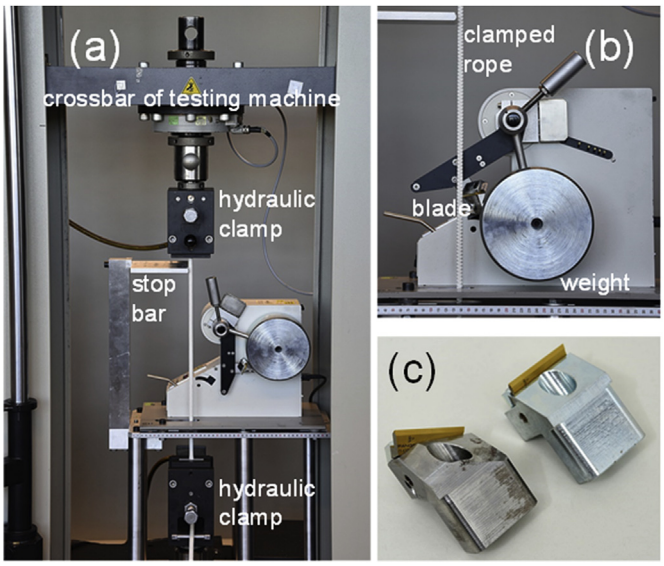

Fig. 3. Experimental setup for cut resistance test: (a) view of modified pendulum tester mounted between the pneumatic clamps of a 100 kN universal testing machine; (b) detail view of pendulum tester modified for the cut resistance test; (c) 0° and 35° blades available for the laboratory cut resistance test.

2.3. Field trials

The field trials were performed at the Competence Center of Alpine Services of the Swiss Armed Forces in Wassen, Switzerland. The central part of the test rig consists of different granite sharp edges in 30° and horizontal configurations (Fig. 4). For the analysis, one end of a rope with a length of 2 m was fixed to a concrete falling mass of 94 kg, while the other end was attached to a piezoelectric load cell (type 9331, 20 kN, Kistler Instrumente, Winterthur, Switzerland) located behind the granite edge. Overhand loop knots were used for both rope ends. The peak force from the load cell was recorded with a charge meter (type 5015, Kistler Instrumente, Winterthur, Switzerland). The concrete mass was lifted to induce a fall length of 1.5 m (fall factor approx. 0.7). The test was initiated using a quick release device (type Fallhaken 2t, Empa, St. Gallen Switzerland). After the rope failed, the falling mass was caught using a double-guided auxiliary rope (Fig. 4a). Each experiment was filmed with two high definition video cameras (type HS900, Panasonic, Kadoma, Japan). The cameras were installed to have a front and top view of the granite edge, at the point where the rope rupture was expected.

2.4. High speed video imaging

A Redlake MotionXtra HG-100K high-speed digital camera with a frame rate of 60,000 frames per second and an image resolution of

Fig. 4. Field trials setup: (a) 94 kg concrete block used as falling mass for cut resistance tests hanging from a safety rope; (b) concrete block attached to test rope, auxiliary rope and remote-controlled quick release device to initiate the test; (c) and (d) close ups of the 30° tilted granite sharp edge on which the test rope slides during the cut resistance test.

128 × 64 pixels was used to video capture the failure of a tensed rope due to contact with a sharp edge.

2.5. Scanning electron microscopy

The modes of failure induced by the cut resistance tests on the ropes were analyzed at the single filament level using a scanning electron microscope (SEM). For this purpose, fiber specimens were carefully extracted from the cut rope specimens using tweezers and scissors. Attention was paid to avoid tampering with the filament ends. The extracted filaments were mounted on a SEM sample holder by pasting them directly onto a double sided carbon tape. The filaments were then sputter coated with the high vacuum film deposition system, Leica EM ACE600, applying a 5 nm gold/palladium coating. The analysis of failure modes was carried out using a Hitachi S-4800 field emission SEM with an accelerating voltage of 2.0 kV and an emission current of 10 μA.

3. Results and discussion

3.1. Laboratory experiments on cut resistance

The effect of pre-tensioning force on the specific energy needed by the pendulum tester to cut the 9.7 mm rope is displayed on Fig. 5a. The trend reported by Bückers [13], in which an increase in pre-tension force leads to a reduction of specific energy needed to cut the rope, is confirmed by the new experimental setup. When the rope is held in tension, considerable stretching ensues and its linear density is thus reduced, where linear density reduction will be proportional to applied tension. As linear density decreases, less energy will be needed to cut the rope. The significant advantage of the current setup with respect to that of Brückers is that the new method is able to apply pre-tension forces of the order of several kN in a reliable and reproducible manner, while the setup of Bückers could only reach a maximum pre-tension value of a few hundred N (Fig. 2) [13]. This aspect is of particular relevance, since the actual load that the human body experiences during a rock climbing fall is in the order of a few kN, where the human body should not be subjected to loads above 12 kN [1,10]. Fig. 5b presents the average specific cutting energy values obtained experimentally for the different dynamic climbing ropes. Although the braiding architecture is not identical for all specimens under consideration and is, therefore, expected to influence cut resistance to some extent, the direct proportionality between the measured specific cutting energy values and rope diameter is very evident for all the ropes subjected to the same type of coating. The coefficient of variation for the cutting energy measurements fluctuated between 9 and 15% for the different rope types under consideration, which was assumed to be an acceptable range based on our experience with several types of fibrous structures. It has been mentioned in the Introduction that one of the main functions of the sheath in a *kernmantle* rope is to protect the load-bearing core from abrasion. Fig. 5c indicates how, when the experimental cutting energy values are normalized by the linear density of the sheath component, a clear correlation with rope diameter is obtained. The influence of sheath density on specific cutting energy is further illustrated in Fig. 5d, where the direct proportionality is unmistakable.

3.2. Analysis of failure modes resulting from the laboratory experiments

Fig. 6 shows the experimental results for two ropes with similar diameters and different hydrophobic coatings (9.5 (ii) and 9.7 mm). Their specific cutting energy values are significantly different. In order to gain a better understanding of the mechanisms influencing cut resistance, filaments extracted from failed specimens of both types of ropes have been analyzed by SEM. Fig. 7a illustrates the cross section of a cut rope and the five distinct regions from which filaments were extracted for the SEM study.

When the blade comes in contact with the tensed rope (region 1 in Fig. 7a), the shearing forces exerted by the tip of the blade flatten and distort the cut filaments (Fig. 8a and d) [16]. Once the first filaments have been cut, yarn mobility in the rope's sheath is enhanced, leading to an increase of frictional forces that generate heat to the point where the skin of some filaments has been softened and distorted (Fig. 8c and f). The combined effects of frictional, shearing and plastic drawing forces generate enough heat to induce some filaments to fuse together (Fig. 8b and e) [16]. Once the blade has cut through the sheath and reaches the core strands (region 2 in Fig. 7a), the pendulum still has a large amount of kinetic energy which is further converted to heat by friction, shear and drawing of filaments. The high speed with which the filaments are cut can be described as an adiabatic process where all heat is used to melt the polymer with no dissipation to the environment, fusing larger amounts of filaments together (Fig. 9a and d). Nevertheless, we note here that the number of filaments fused together in the 9.5 mm rope (Fig. 9d) is considerably smaller than in the 9.7 mm rope (Fig. 9a), indicating a lower temperature in the former rope. This is consistent with what we find in Fig. 9c and f, where we see that single filaments in the 9.7 mm rope have been fully melted, while the filaments in the 9.5 mm rope, although showing the

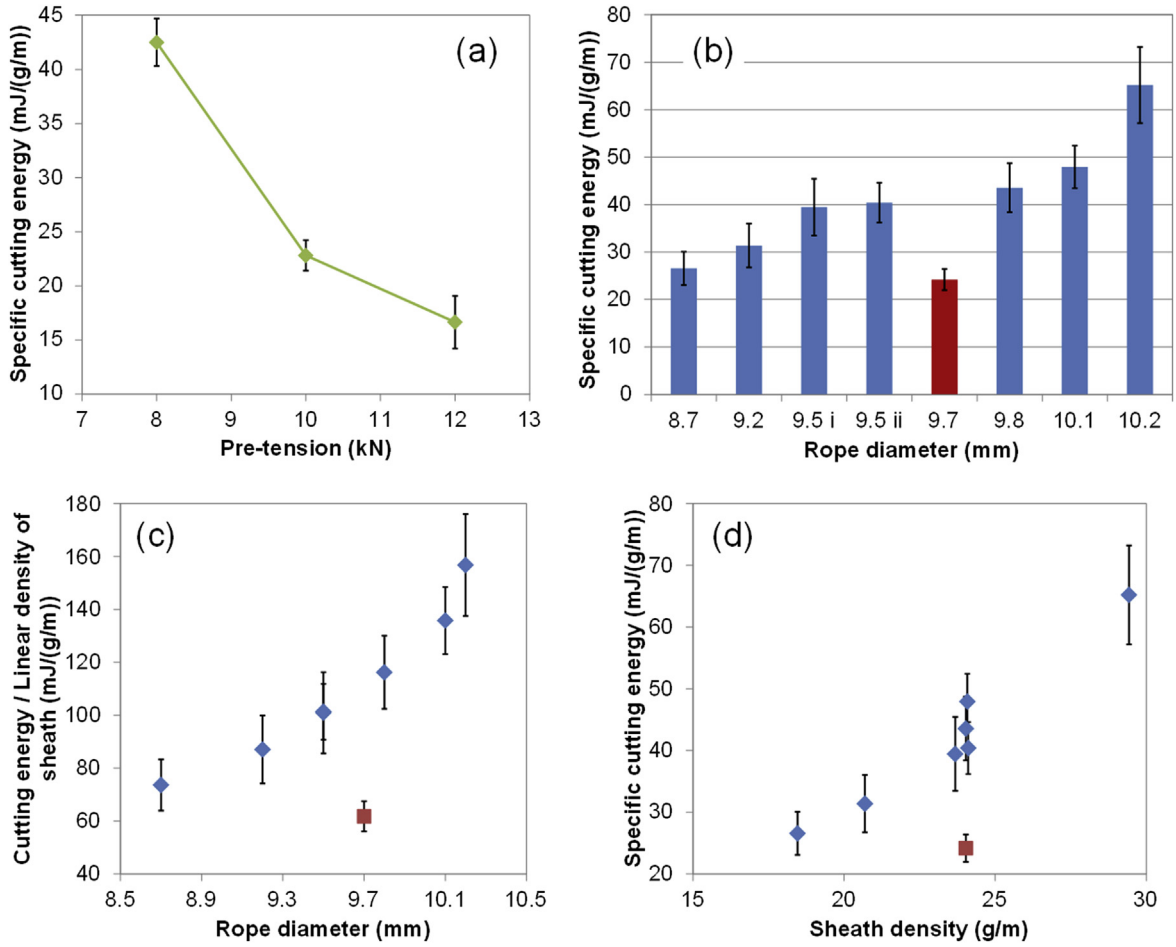

Fig. 5. (a) Effect of pre-tensioning force on the specific energy needed to cut the 9.7 mm diameter rope; (b) correlation between specimen diameter and specific cutting energy; (c) correlation between specimen diameter and cutting energy normalized by the linear density of the rope's sheath component; (d) influence of sheath linear density on specific cutting energy. The 9.7 mm rope received a different hydrophobic coating than the rest of the ropes under analysis. A pre-tension of 10 kN was used in (b), (c) and (d). The lines joining the data points in (a) serve only as a visual aid. All error bars represent ± one standard deviation.

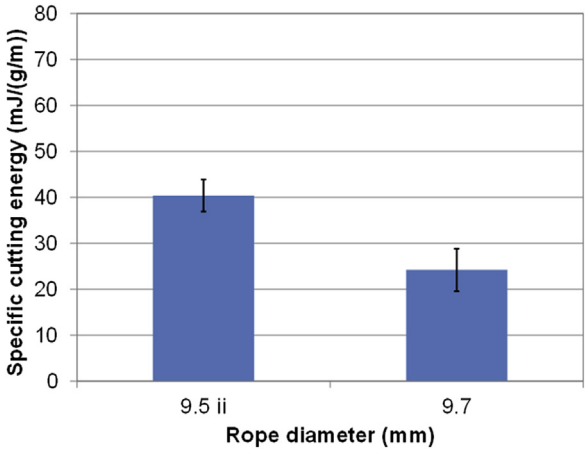

Fig. 6. Specific cutting energy of ropes used for the analysis of failure modes (pre-tension 10 kN). The ropes were produced using different hydrophobic coatings.

influence of heat, are able to retain their original shape. The flattening and distortion of single filaments as they come in contact with the blade is still visible (Fig. 9b and e).

The analysis of filaments extracted from regions 3 and 4 (Fig. 7a) of tested rope specimens demonstrates that, at this stage of the test, the main mode of deformation is high speed tensile loading. All specimens analyzed in these regions for both ropes under consideration show classical mushroom failed ends (Fig. 10). When the filaments break under tension, the elastic energy stored in the fiber regions neighboring the point of failure causes recoil of both fiber ends. Once the recoil is completed, the heat-softened polymer collapses into a mushroom shape [17,18]. High-speed video recordings of rope failure due to contact with a sharp edge confirm this mode of failure. Video 1 illustrates how, once the sheath has been fully severed, the core strands furthest away from the initial point of contact with the blade (i.e. the strands in regions 3 and 4) remain undamaged for a few milliseconds. Given that these few strands must still support the 10 kN pre-tension, high speed tensile failure ensues. Finally, looking at the SEM images of filaments extracted from the sheath originally furthest away from the blade (region 5 in Fig. 7a), we find flattened and distorted broken ends for both ropes (Fig. 11a and d) just as in region 1 discussed above. The argument made in the discussion of SEM micrographs for region 2, where the rope with better cut resistance appears to be exposed to smaller amounts of heat during the cutting event than its counterpart, is confirmed in Fig. 11, where the broken ends extracted from the 9.7 mm rope with inferior cut resistance exhibit more intensive recoil damage (Fig. 11b) and skin distortion (Fig. 11c) than those revealed by the 9.5 mm rope with improved cut resistance (Fig. 11e and f). In summary, the failure modes illustrated in

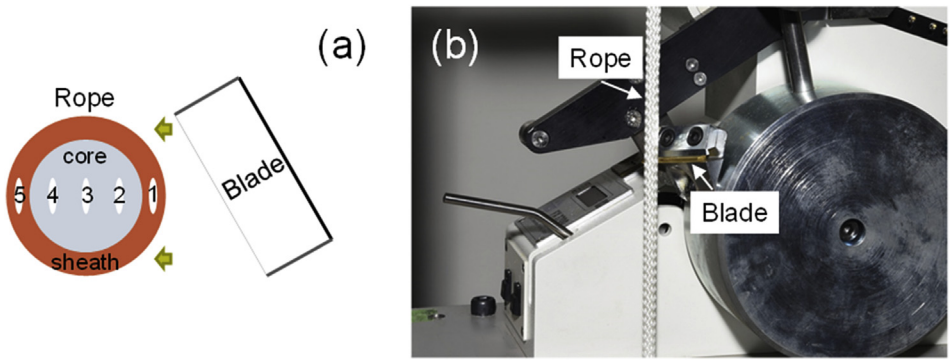

Fig. 7. (a) Schematic of incoming blade and rope cross section showing the five distinct regions from which specimens were extracted for analysis after the rope was cut; (b) actual view on the testing machine.

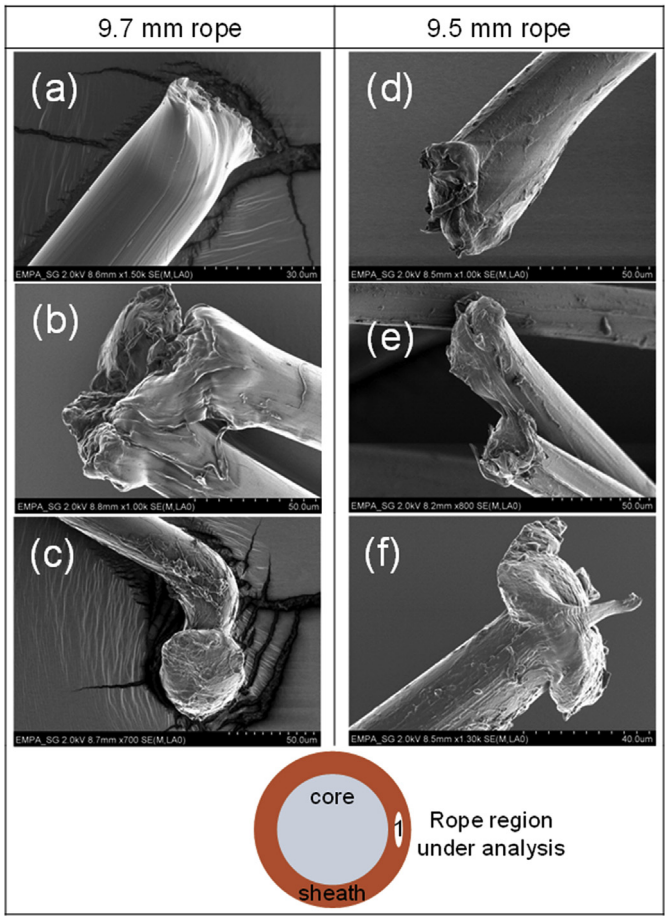

Fig. 8. SEM micrographs of filaments extracted from rope region 1 after cut resistance testing in the laboratory for (a–c) the 9.7 mm and (d–f) the 9.5 mm ii ropes.

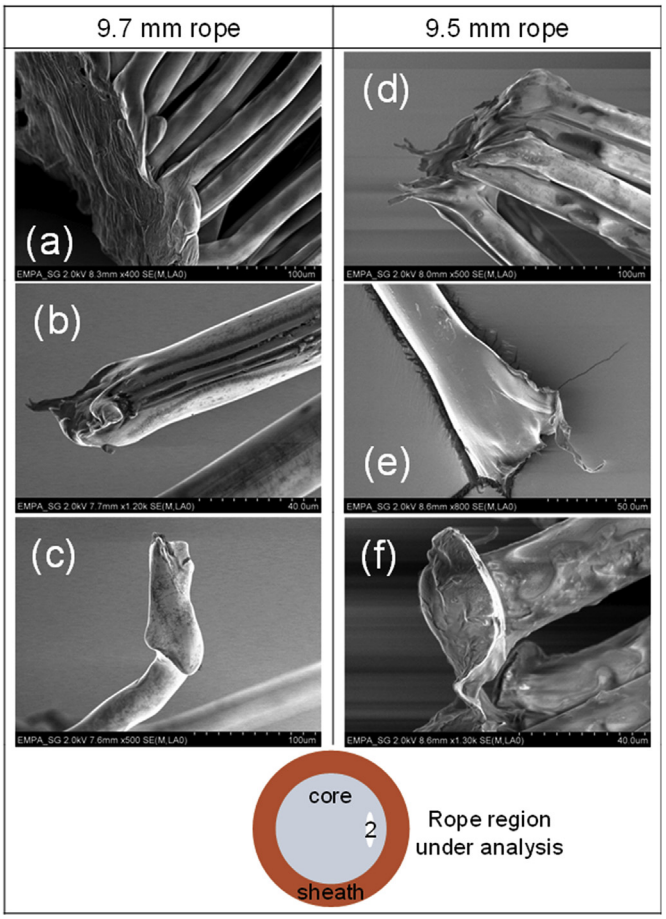

Fig. 9. SEM micrographs of filaments extracted from rope region 2 after cut resistance testing in the laboratory for (a–c) the 9.7 mm and (d–f) the 9.5 mm ii ropes.

Fig. 8–11 indicate that the more localized frictional heating a climbing rope suffers during a cutting event, the less cut resistance it will achieve.

Supplementary video related to this article can be found at http://dx.doi.org/10.1016/j.polymertesting.2017.07.004.

3.3. Field trials

Field trials have been performed on the 30° granite sharp edge shown in Fig. 4c and d using the 8.7, 9.5 ii and 10.2 mm ropes. A typical test where the rope fails instantly can be seen in Video 2. All tested specimens for the 8.7 mm rope failed instantly upon contact with the sharp edge, whereas only 55% of the 9.5 mm specimens and none of the 10.2 mm specimens followed this behavior. In contrast, 27% of the 9.5 mm specimens and 77% of the 10.2 mm specimens were not severed during the experiment. Fig. 12b shows how as the maximum specific force applied on the rope during the fall increases, as does the probability that the rope will fail due to contact with a sharp edge. The practical relevance of the laboratory experiments discussed in section 3.1 and Fig. 5 is confirmed in

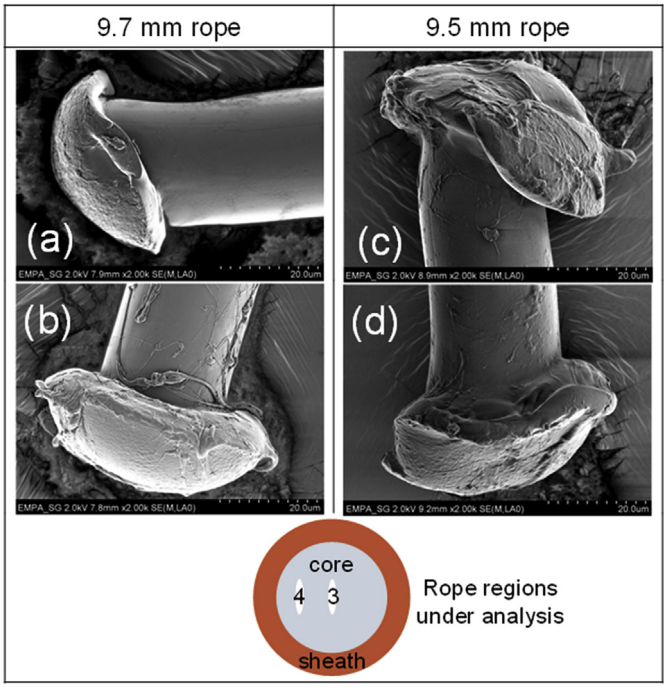

Fig. 10. SEM micrographs of filaments extracted from rope regions 3 and 4 after cut resistance testing in the laboratory for (a–b) the 9.7 mm and (c–d) the 9.5 mm ii ropes.

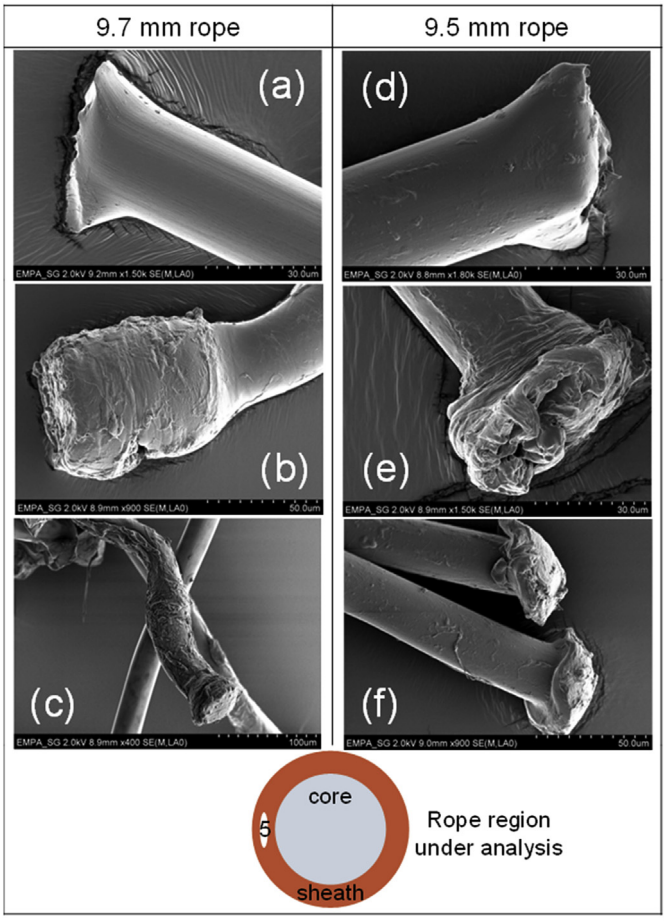

Fig. 11. SEM micrographs of filaments extracted from rope region 5 after cut resistance testing in the laboratory for (a–c) the 9.7 mm and (d–f) the 9.5 mm ii ropes.

Fig. 12c, where a very strong correlation between specific maximum force measured in the field trials and specific cutting energy measured in the laboratory is observed. The rope with the lowest specific cutting energy values in the laboratory always failed in the field trials, while the rope with the highest laboratory values always survived the field trials.

Supplementary video related to this article can be found at http://dx.doi.org/10.1016/j.polymertesting.2017.07.004.

An SEM analysis of filaments extracted from the 9.5 mm ropes tested in the field trials is summarized in Fig. 13 and Fig. 14. Comparing it against the modes of failure reported in Section 3.2 for the specimens tested in the laboratory, it is found that all failure modes induced by the laboratory setup are also encountered in the field trial specimens: flattening and distortion (Fig. 13b and d, Fig. 14a and d), skin softening (Fig. 13c), fusing together of neighboring filaments (Fig. 14b) and mushrooms caused by high speed tensile failure (Figs. 13a and 14c). It is interesting to note that filaments fused together have been found throughout the entire cross section of the field trial specimens. This is in contrast with the laboratory experiments, where filaments fused together were only found in the cross section regions 1 (Fig. 8) and 2 (Fig. 9). This observation indicates that testing in the field trial configuration introduces a larger amount of heat in the rope than the laboratory setup, which is representative of the difference in potential energy available in each test. The failure mode encountered in Figs. 13e and 14f in which a fiber is continuously damaged throughout a length in the order of 300 μm is not found in the specimens tested in the laboratory and is due to the larger length of rope that comes in contact with the tilted sharp edge in the field trials, as opposed to the very localized damage caused by the blade in the laboratory experiments. Finally, the field trials also induce a very intriguing mode of failure depicted in Figs. 13f and 14e. This type of failure is the result of a very complicated mode of deformation which involves simultaneous bending and twisting of the fiber [17,19]. Goswami and Hearle have been able to reproduce this type of failure mode in the laboratory by bending a fiber around a pin fixed perpendicularly to the fiber axis, while one end of the fiber is clamped statically and the other end is rotated [20]. Under this state of loading, the twist flow induced by the rotation of one fiber end is halted at the point of contact between the fiber and the pin, inducing abrasion which in turn heats up the fiber which is already being subjected to tensile, compressive and shearing forces [20]. Similarly, in the case of the climbing rope being tested in the field trials, any rotation introduced in the rope by the falling mass as the rope slides over the tilted sharp edge will be arrested at the point of contact between rope and sharp edge, introducing simultaneous bending and twisting loads on the rope at the point of contact, along with abrasion. Such a complex state of loading cannot be reproduced by the laboratory test device developed in this work due to the restrictions imposed by the fixed-fixed rope clamping conditions. Nevertheless, the discussion of failure modes obtained in the laboratory and in the field confirms the practical relevance of the developed methodology for the laboratory quantification of cut resistance in dynamic climbing ropes.

4. Conclusions

The combined use of a modified Elmendorf tear tester and a universal tensile testing machine has enabled the development of a test method which applies pre-tension forces to the rope in the order of several kN during the cut resistance test. This results in a reliable and reproducible testing methodology which is able to mimic the state of loading endured by the rope during a real life rock climbing event. The SEM analysis of specimens tested both in laboratory and in field trials demonstrates the same modes of

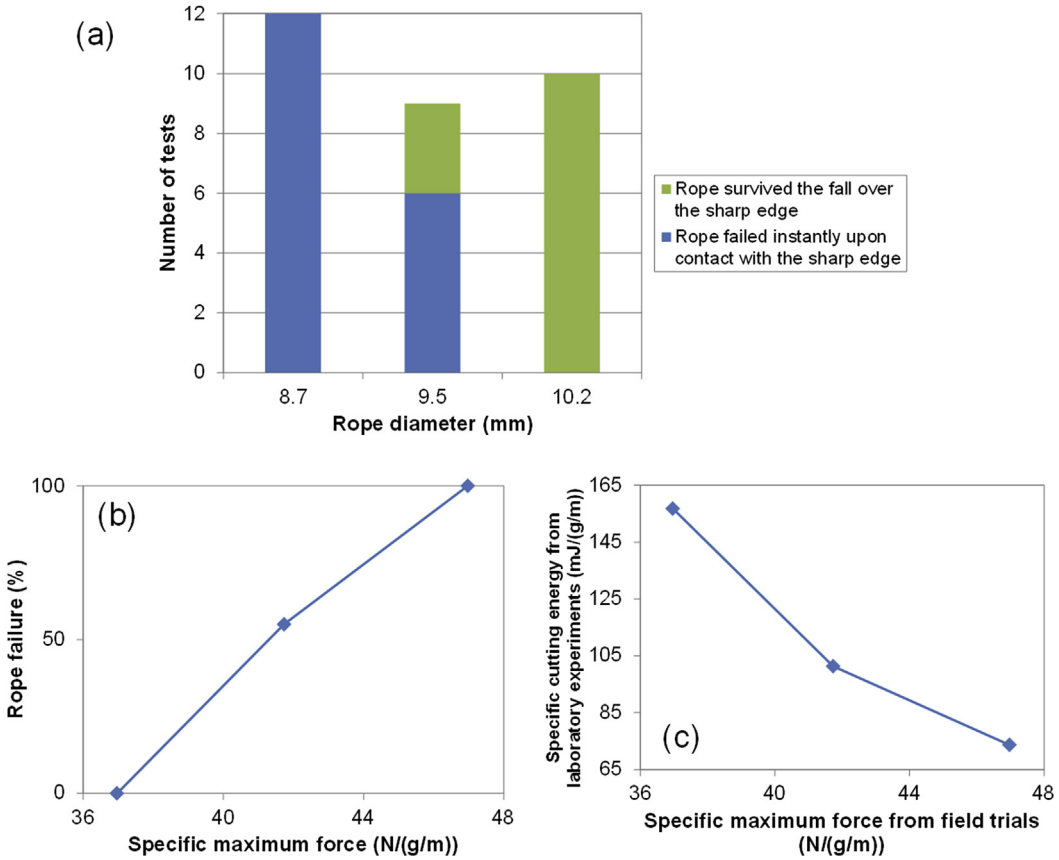

Fig. 12. Field tests results: (a) stacked histogram of qualitative results produced by the field trials; (b) rope failure as a function of measured specific maximum force applied on the climbing rope during a fall over the tilted granite sharp edge; (c) correlation between measurements obtained in field trials and laboratory experiments. The lines joining the data points in (b) and (c) serve only as a visual aid.

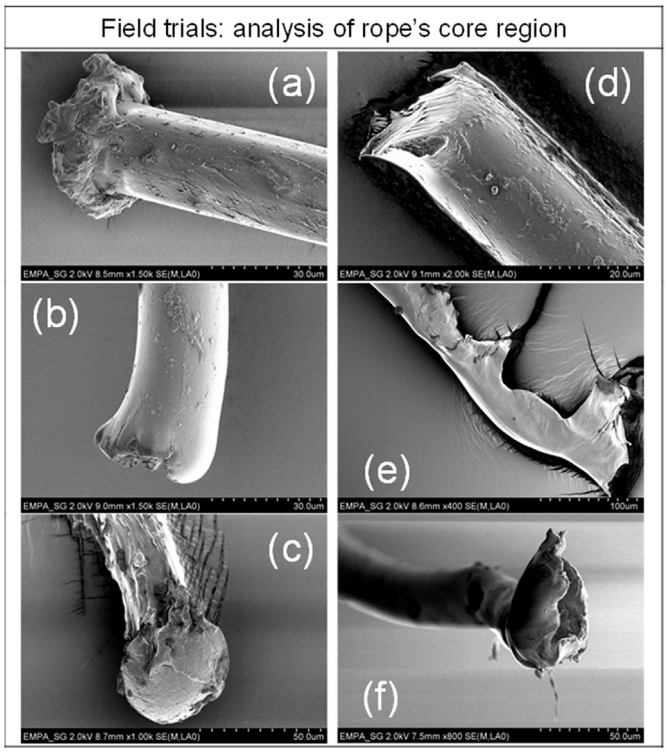

Fig. 13. SEM micrographs of filaments extracted from the core region of ropes subjected to field trials.

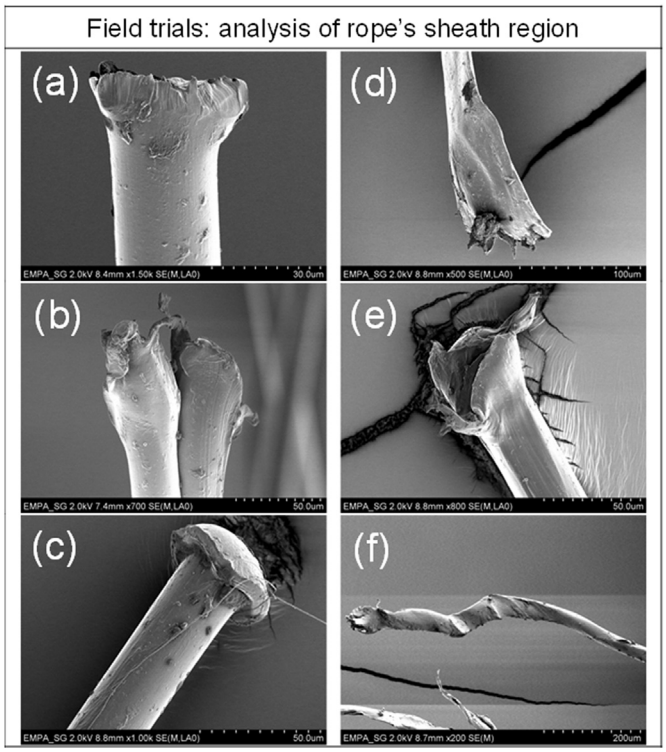

Fig. 14. SEM micrographs of filaments extracted from the sheath region of ropes subjected to field trials.

failure of the filaments composing the rope as it comes in contact with the sharp edge: flattening and distortion, skin softening, fusing together of neighboring filaments and mushroom-shaped fiber ends. The microscopy analysis also confirms that cut resistance is associated with the ability of the rope to diminish the generation of heat during the cutting event.

One of the driving factors in developing rock climbing equipment is weight reduction which, in case of climbing ropes, leads to a trend towards products with smaller diameters. Such ropes might still show excellent performance to protect climbers against normal falls, but the reduced safety reserve affects cut resistance. A maximization of the performance to weight ratio has led to a situation in which every filament in the rope is exposed to a considerable amount of mechanical load during climbing, making the rope vulnerable to the propagation of failure once one or a few filaments in the tensed rope have been cut. In recent decades, a vast majority of the fatal climbing accidents due to rope failure were caused by cutting against a sharp edge [21]. With the development of a reliable and reproducible testing procedure to quantify rope cut resistance, we believe to have laid the base for a substantial safety increase in mountaineering activities.

Acknowledgements

The authors wish to acknowledge Ernst Rüegg and Jörg Gschwend for their support with the design and construction of the cut resistance testing device. Marcel Halbeisen, Pier-Luigi Barbadoro and Joel Gächter are acknowledged for their help in carrying out the testing of the ropes and for capturing the high-speed videos. Markus Hilber and Olivia Neururer are also acknowledged for their help with rope testing. Roger Würsch and the Competence Center of Alpine Services of the Swiss Armed Forces are acknowledged for their support in performing the field trials. Mammut Sports Group AG is acknowledged for supplying the ropes used for testing and analysis.

Funding: This work was supported by the Commission for Technology and Innovation (CTI) of the Swiss Federal Administration [grant number 16927.1 PFIW-IW].

References

[1] A.J. McLaren, Design and performance of ropes for climbing and sailing, Proc. Inst. Mech. Eng. Pt. L-J. Mater.-Design Appl. 220 (2006) 1–12.
[2] N. Pan, D. Brookstein, Physical properties of twisted structures. II. Industrial yarns, cords, and ropes, J. Appl. Polym. Sci. 83 (2002) 610–630.
[3] M. Pavier, Derivation of a Rope Behaviour Model for the Analysis of Forces Developed during a Rock Climbing Leader Fall, A a Balkema, Rotterdam, 1996.
[4] C.M. Leech, The modelling of friction in polymer fibre ropes, Int. J. Mech. Sci. 44 (2002) 621–643.
[5] C.M. Leech, J.W.S. Hearle, M.S. Overington, S.J. Banfield, Modelling tension and torque properties of fibre ropes and splices, in: Proceedings of the Third (1993) International Offshore and Polar Engineering Conference, 1993, pp. 370–376.
[6] J.B. Mayo, E.D. Wetzel, Cut resistance and failure of high-performance single fibers, Text. Res. J. 84 (2014) 1233–1246.
[7] M. Hudspeth, D.W. Li, J. Spatola, W.N. Chen, J. Zheng, The effects of off-axis transverse deflection loading on the failure strain of various high-performance fibers, Text. Res. J. 86 (2016) 897–910.
[8] H.S. Shin, D.C. Erlich, J.W. Simons, D.A. Shockey, Cut resistance of high-strength yarns, Text. Res. J. 76 (2006) 607–613.
[9] M. Pavier, Experimental and theoretical simulations of climbing falls, Sports Eng. 1 (1998) 79–91.
[10] M. Rüedi, R. Stämpfli, R. Gross, Statische und dynamische Prüfungen von Seilen und Gurten, Euroseil 118 (1999) 503–506.
[11] M. Blümel, Scharfkantenprüfung von Bergseilen, Department of Sport and Health Sciences, Technical University of Munich, Munich, Germany, 2005, p. 122.
[12] M. Blümel, V. Senner, H. Baier, Development of a sharp edge resistance test for mountaineering ropes, Impact Technol. Sport II (2008) 701–706. Singapore.
[13] M. Bückers, Kantenarbeitsvermögen von Kern-Mantel-Materialien aus dem Bergsport, Department of Sport and Health Sciences, Technical University of Munich, Munich, Germany, 2010, p. 81.
[14] A.B. Spierings, A. Ritter, O. Henkel, U. Holzdoerfer, Investigation of the water repellence of different experimental and commercial coatings for synthetic mountaineering ropes, Text. Res. J. 78 (2008) 886–895.
[15] DIN EN 892:2012+A1:2016, Mountaineering equipment - Dynamic mountaineering ropes - Safety requirements and test methods.
[16] J.W.S. Hearle, B. Lomas, W.D. Cooke, Ropes, Atlas of Fibre Fracture and Damage to Textiles, CRC Press LLC, Boca Raton FL, 1998, pp. 336–358.
[17] J.W.S. Hearle, Forms of Fibre Fracture, Elsevier Science Bv, Amsterdam, 2002.
[18] J.W.S. Hearle, B. Lomas, W.D. Cooke, High-speed Tensile Break, Atlas of Fibre Fracture and Damage to Textiles, CRC Press LLC, Boca Raton FL, 1998, pp. 50–51.
[19] J.W.S. Hearle, B. Lomas, W.D. Cooke, Miscellany, Atlas of Fibre Fracture and Damage to Textiles, CRC Press LLC, Boca Raton FL, 1998, pp. 163–172.
[20] B.C. Goswami, J.W.S. Hearle, Comparative study of nylon fiber fracture, Text. Res. J. 46 (1976) 55–70.
[21] C. Hummel, F. Hellberg, Weisst du, wo die Kante lauert, Dav. Panor. (2016) 56–59.